

An evaluation of LES for jet noise prediction

By B. Rembold[†], J. B. Freund[‡] AND M. Wang

Large-eddy simulation (LES) is an attractive candidate for prediction of jet noise, since it resolves unsteady flow structures over a range of length scales, but it remains unclear how the subgrid-scale modeling affects its noise-prediction capability. The present study makes a direct evaluation of LES using the approximate deconvolution model against a corresponding direct numerical simulation (DNS) of a 5:1 aspect ratio rectangular jet at Mach 0.5. The DNS spectra and directivity are as anticipated for a low-Reynolds-number jet, and we compare these to LES predictions. We find that the LES spectra match the DNS ones at low frequencies, but the higher frequency portions are highly contaminated by spurious waves particularly at upstream angles. A correction for the subgrid-scale contribution to the Lighthill source terms based on approximate deconvolution of the velocities does not change the LES prediction.

1. Introduction

The success of efficient RANS models in fluids engineering has not extended to the prediction of noise, even when the only objective is to predict general trends, and it is not obvious how to improve their fidelity given the complexity of statistical noise sources. Since the inherent flow unsteadiness is the source of jet noise, LES is attractive for its prediction. The computation of flow induced noise has its unique difficulties, and several important issues arise when extending an established DNS capability, which of course is only applicable in the low-Reynolds-number limit (*e.g.* Freund 2001), to noise. With LES additional questions, such as the effects of subgrid-scale modeling and numerical errors, must be addressed.

LES can be most easily applied if the bulk of the noise, at least at frequencies of interest, comes from scales that are retained in the simulation, and do not have to be modeled. This is believed to be the case based on statistical analysis, and it seems that high-frequency noise does indeed come from the vicinity of the jet nozzle (Narayanan, Barber & Polak 2000). One objective of this study is to confirm that LES can predict the louder, lower-frequency noise. Another objective is to see if the subgrid-scale turbulence models directly affect the noise prediction. The subgrid-scale stress terms in the spatially filtered Navier-Stokes equations are closed by a model, which also appears as a noise source but is not necessarily accurate. Their effects on the resolved scales thus need to be evaluated. Discretization errors can also play a larger role in LES than in DNS since the spectra are typically truncated by the mesh at a much higher energy level, which is another potential problem for LES of jet noise. Thus, we also investigate a spurious generation of noise by numerical errors. A long-term objective is to correct this spurious effect.

To investigate these issues we use DNS results for a rectangular jet with Mach number

[†] Institute of Fluid Dynamics, ETH Zürich

[‡] Department of Theoretical and Applied Mechanics, University of Illinois at Urbana-Champaign

0.5 and Reynolds number 2000 (based on the shorter dimension of the nozzle) rectangular jet (Rembold, Adams & Kleiser 2002). Rectangular jets are of current interest because in some cases they are quieter than their axisymmetric counterparts. They also have enhanced mixing properties (Grinstein 2001), which is important in some military applications. A previous LES study by Rembold, Adams & Kleiser (2001) using the approximate deconvolution subgrid-scale model (Stolz & Adams 1999, Stolz, Adams & Kleiser 2001) showed turbulence statistics in agreement with the DNS in the transition region, but the jet's noise was not computed. In this study we use Lighthill's theory to compute the far-field noise, and compare the noise predicted using the DNS and LES source terms. Our formulation of Lighthill's theory is outlined in section 2. Section 3 covers the results from the DNS database, and comparisons between LES and DNS are made in section 4.

2. Far-field sound computation

Lighthill's equation reads

$$\frac{\partial^2 \rho}{\partial t^2} - c_0^2 \frac{\partial^2 \rho}{\partial x_i \partial x_i} = \frac{\partial^2 T_{ij}}{\partial x_i \partial x_j} \quad , \quad (2.1)$$

with

$$T_{ij}(\mathbf{x}, t) = \rho u_i u_j + \delta_{ij} \{p - p_0 - c_0^2(\rho - \rho_0)\} - \tau_{ij}. \quad (2.2)$$

Here $\tau_{ij} = \mu \left(\frac{\partial u_i}{\partial x_j} + \frac{\partial u_j}{\partial x_i} - \frac{2}{3} \delta_{ij} \frac{\partial u_k}{\partial x_k} \right)$ is the viscous stress tensor. Taking $\frac{\partial^2 T_{ij}}{\partial x_i \partial x_j}$ as the equivalent noise source, the far-field sound at point \mathbf{x} is evaluated using the free space Green's function and the divergence theorem as

$$\rho(\mathbf{x}, t) = \frac{1}{4\pi c_0^4} \int_V \frac{R_i R_j}{R^3} \frac{\partial^2}{\partial t^2} T_{ij}(\mathbf{y}, t - \frac{R}{c_0}) d\mathbf{y}, \quad (2.3)$$

where $R = |\mathbf{x} - \mathbf{y}|$ and $R_i = x_i - y_i$. Evaluation is simplified by reformulating (2.3) in frequency space in dimensionless form, as

$$\rho(\mathbf{x}, \omega) = \frac{M^4}{4\pi} \int_V \frac{R_i R_j}{R^3} \omega^2 T_{ij}(\mathbf{y}, \omega) e^{-iMR\omega} d\mathbf{y}, \quad (2.4)$$

since this avoids the interpolation needed to compute retarded times in (2.3). Both formulations correctly represent the quadrupole nature of the source, and have been shown to facilitate an accurate numerical evaluation (Bastin, Lafon & Candel 1997). The variables are non-dimensionalized using jet exit quantities and $L_1/2$ defined in figure 1. In evaluating (2.4) we neglect τ_{ij} which is typically small (Goldstein 1976). The second term in the tensor is also small in nearly-isentropic flow, and so is also expected to be small here. Thus for the present analysis we retain only $\rho u_i u_j$ in the source tensor.

3. DNS results

3.1. Database description

The coordinate system and a visualization of the jet simulation are shown in figures 1 and 2, respectively. Relevant physical and computational parameters are listed in table 1. A high-order compact finite-difference algorithm was used to solve the compressible Navier-Stokes equations in Cartesian coordinates; it is fully discussed by Rembold *et al.* (2002).

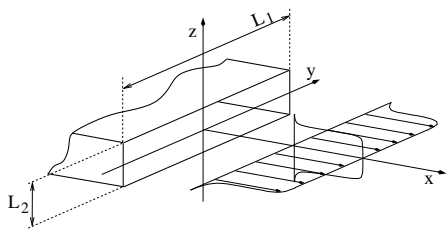


FIGURE 1. Inflow profile and coordinate system

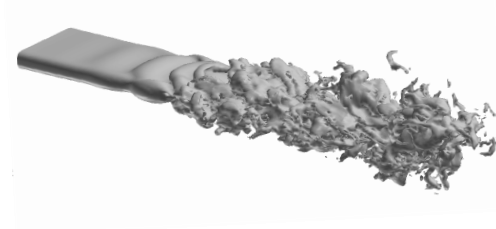


FIGURE 2. Flow topology visualized by density isosurface

L_1/L_2	5
$Re_{L_1/2,j}$	5000
M_j	0.5
T_∞/T_j	0.936143
Strouhal Number ($= L_1 \pi f / u_j$)	2.7066
grid (x, y, z)	$337 \times 229 \times 229$
box	$(15 \times 14 \times 14) L_1/2$
computational time	78.8
time samples used	552
average sampling interval	0.1435

TABLE 1. Parameters of the jet DNS database. The subscript j denotes jet-center quantities. Unless noted, quantities are non-dimensionalized by ρ_j , u_j , and $L_1/2$.

A smoothed laminar top-hat velocity profile, as suggested by Yu & Monkewitz (1990),

$$u(\eta, \zeta) = \frac{1}{(1 + \sinh[|\eta| \sinh^{-1}(1)]^{2n_1}) (1 + \sinh[|\zeta| \sinh^{-1}(1)]^{2n_2})} \quad (3.1)$$

defined the inflow, where η and ζ are the cross-stream coordinates normalized by the corresponding velocity half-width $L_i/2$, $i = 1, 2$. The parameters $n_1 = 9$ and $n_2 = n_1 L_2/L_1$ gave a common vorticity thicknesses $\delta = \delta_i = L_i / [\sqrt{2} n_i \sinh^{-1}(1)]$ in both directions. A linearly-unstable eigenmode was superimposed on this inflow at $St = 2.7066$ in order to trigger transition.

A total of 552 samples in time (dimensionless time interval 78.8) of the full DNS fields were used to compute the sound sources. This set was subdivided into sub-intervals of five overlapping sets of 192 samples each. The Lighthill stress tensor was computed in each interval, and time transformed using a discrete Fourier transform. The samples were windowed in time using a function constructed from a half-period of a cosine function, which ramped the signal smoothly to zero over 50 samples at the beginning and end of each window to reduce spurious high frequencies introduced by the finite sample length. Figure 3 shows a windowed fluctuation pressure signal at $y = z = 0$, $x = 6.2$. The data was unfortunately stored at non-equidistant intervals, but the change of the interval length was less than one percent, and the associated error in the evaluation of Fourier sums was shown to have negligible consequence for the frequencies of interest.

The far-field sound spectra were obtained by numerical evaluation of (2.4) using trapezoidal rule quadrature. The source term T_{ij} goes to zero at large y and z and at the inflow boundary, which allows integrating all the way to the domain boundaries. At the outflow

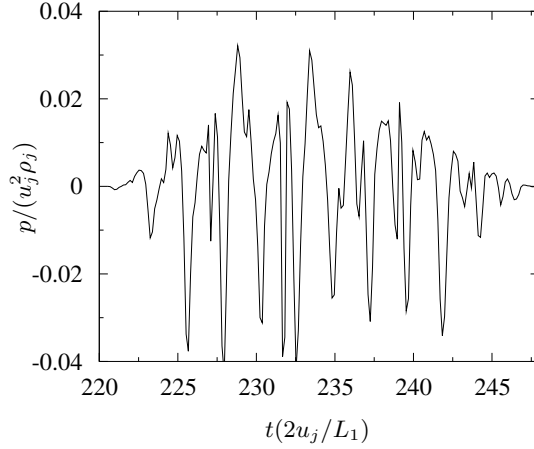


FIGURE 3. Pressure fluctuation signal at sensor point on the jet-center-axis in the transition region of the DNS field.

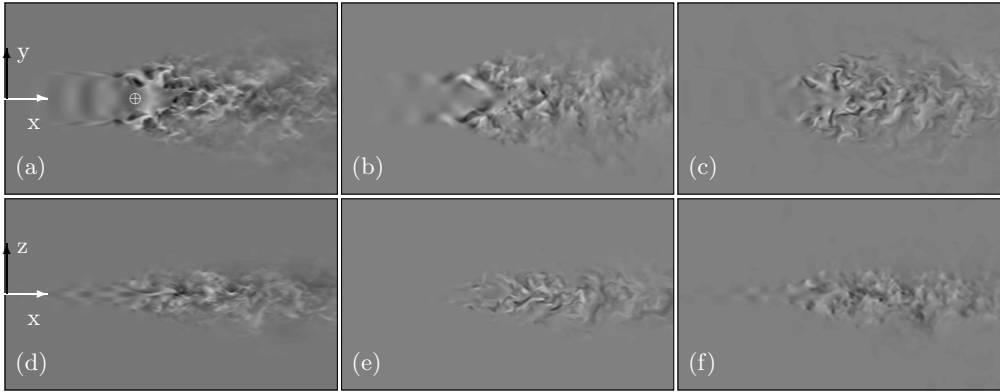


FIGURE 4. Instantaneous contours of T_{11} (a,d), T_{12} (b,e) and T_{13} (c,f) in the major (a-c) and minor (d-f) jet-plane, \oplus origin of the far-field arcs.

boundary it is also small compared to its size in the transition area, though not zero since turbulent structures leave the domain. We therefore smoothly ramped down the source terms close to the outflow boundary in order to avoid affecting the volume integral by leaving sources. It was found that the influence on the particular form of the smoothing function is weak and therefore the same window function as in time was applied.

3.2. Acoustic analysis

In order to visualize the location and structure of the sound sources we plot in figure 4 contours of the dominant source tensor components T_{11} , T_{12} , T_{13} in the two jet-center planes. Here the flow is from left to right and in streamwise direction the entire physical domain is shown. In the lateral directions only the part with significant source terms is shown. From this visualization we see that the maximum source terms are obtained at

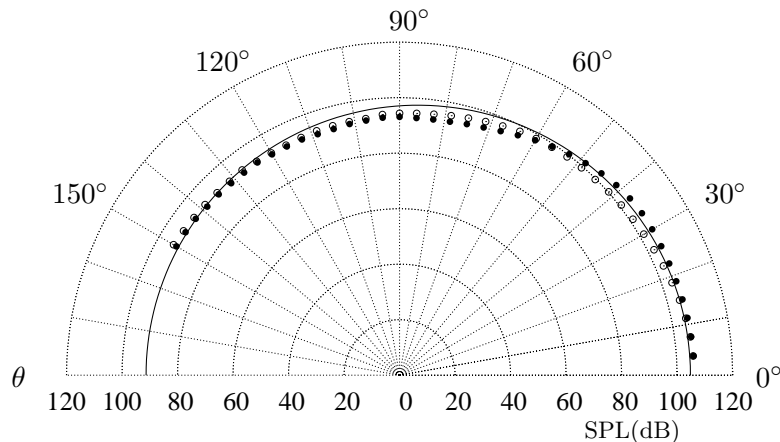


FIGURE 5. Sound pressure level along an arc of radius $60L_1/2$ around the transition area in the major \circ and minor \bullet jet-planes; expected Doppler-scaling — .

the edges of the jet around the location where the potential core closes. The location of the peak of the source does not necessarily coincide with the virtual origin of the radiated sound, since most of the components do not radiate to the far-field. This was shown by Freund (2001), who actually filtered the source terms in order to only obtain the radiating components. However, it does give the indication that the dominant noise producing structures are located in the transitioning shear layers. Far-field spectra and intensities were computed on two arcs in the $y = 0$ and $z = 0$ planes at a radius of $60L_1/2$ and with angle θ measured from the downstream axis. The center of the arcs $x = 5, y = 0, z = 0$ is labeled in figure 4 (a). In figure 5 the radiated sound-pressure-level, $SPL = 10 \log_{10}(p'^2/p_{ref}^2)$, is plotted for the two arcs, taking the standard dimensional reference condition $p_{ref} = 2 \times 10^{-5} Pa$. The anticipated directivity based on a Doppler scaling

$$SPL \sim \frac{1}{(1 - M_c \cos(\theta))^5} \quad (3.2)$$

with assumed convective Mach number $M_c = 0.6M$ is also plotted.

We observe a directivity of the jet peaking near $\theta = 35^\circ$. At this angle, the SPL in the major jet-plane is 5dB lower than that in the minor jet-plane. This effect is reversed at $\theta = 75^\circ$. This trend is consistent with experiments of non-axisymmetric jets which typically show that noise is more directive in the minor plane (Kinzie & McLaughlin 1999), although we note that these observations are for supersonic jets. The overall directivity matches well with the expected directivity for uniformly moving sound sources.

Figure 6 shows noise spectra, $(pp^*)^{1/2}/\rho_j u_j^2$, at six angles for each of the two arcs. The spectra are highly peaked, as expected for a forced low-Reynolds-number jet. At $\theta = 5^\circ$, the two spectra nearly coincide, which is not surprising since the observation points are very close at low angles to the jet. For $\theta = 30^\circ$, the spectrum in the minor plane is slightly higher at most frequencies. By $\theta = 150^\circ$, the spectra are flatter and now not dominated by the forced instability frequency. We observe a slight increase of the far-field spectrum at the high frequency end in this case, which is unphysical. This

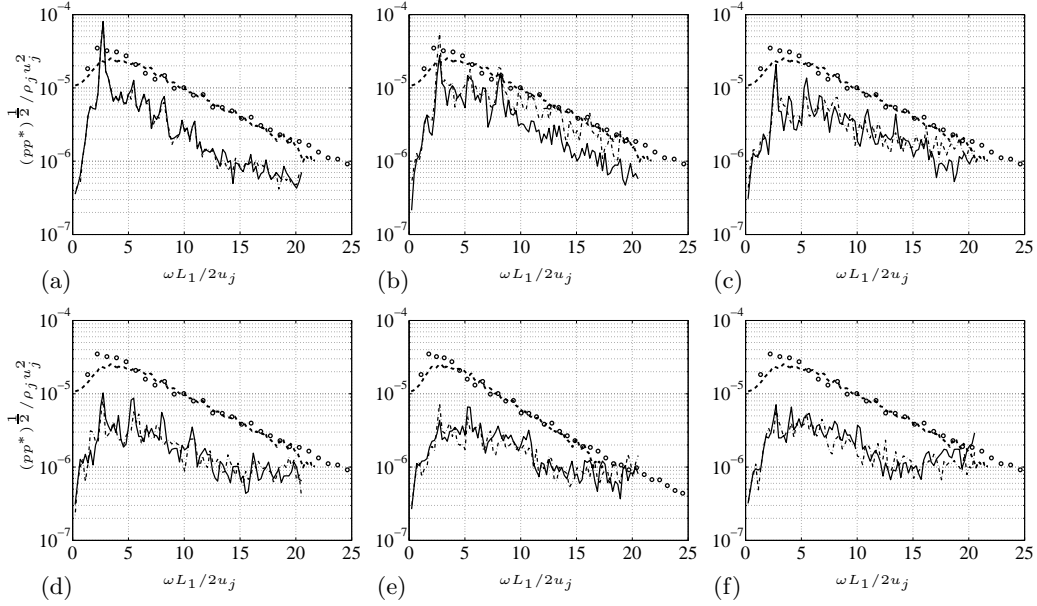


FIGURE 6. Far-field spectra for different θ ($((\cdot))^*$ denoted complex conjugate quantities). $\theta =$ (a) 5° , (b) 30° , (c) 60° , (d) 90° , (e) 120° , (f) 150° , on the arc at radius $60L_1/2$ in the major — and minor — jet-planes. Also plotted are the spectra from a round jet DNS (Freund 2001) \circ and experiments of Stromberg *et al.* (1980) ---- at $\theta = 30$ degrees.

might be caused by the non-equidistant time steps which was neglected in the sound analysis and is being investigated further. For comparison we also plot for all angles the far-field spectrum (arbitrary units) of the DNS data of Freund (2001) and experiments of Stromberg, McLaughlin & Troutt (1980) at an angle of 30 degrees. If the Strouhal number is scaled such that L_2 corresponds to the jet diameter, the drop-off in the spectra matches the present data.

4. LES results

4.1. LES database

The physical parameters of the LES match the DNS. The flow was computed using the approximate deconvolution model, as described in Stolz *et al.* (2001) and Rembold *et al.* (2001) on a $141 \times 77 \times 77$ mesh, which corresponds to one-third the DNS mesh in each direction. We found, however, it necessary to increase the size of the downstream absorbing “sponge” layer over that used in the DNS to suppress reflections from the outflow plane (streamwise thickness of the sponge in DNS is $1.6L_1/2$, compared with $4.8L_1/2$ in LES). The simulation parameters are listed in table 2. Note that for the LES we used constant time steps, and the temporal sampling rate was approximately 1.5 times that of the DNS. Temporal windowing of the same form as for the DNS was applied to the entire data set. In figure 7 we show the analogous pressure-fluctuation signal at a sensor point in the transition region of the jet with the temporal window function

grid (x, y, z)	$141 \times 77 \times 77$
box	$(18 \times 14 \times 14) L_1/2$
computational time	90
samples used	1000
sampling interval	0.09

TABLE 2. Parameters of the jet LES database.

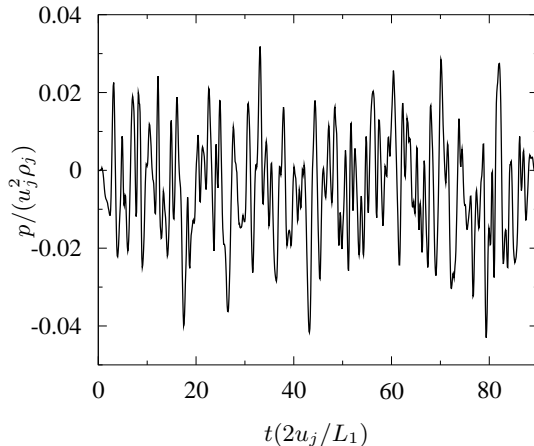


FIGURE 7. Pressure fluctuation signal at sensor point on the jet-center-axis in the transition region of the LES field.

applied. Instead of ensemble-averaging over several sub-samples, spectral binning, which like windowing is a rigorous means of reducing variance, was applied to smooth the spectra. A bin width of $\Delta\omega = 0.35$ was used. The spectra and far-field sound were computed in exactly the same way as for the DNS.

4.2. Acoustic analysis

Naturally, in LES only filtered quantities are directly available for computation of the Lighthill source, although deconvolution potentially offers a means of correcting this. In the approximate deconvolution model, an approximate inverse of the filter is used to partially recover unfiltered data, which is then used to model subgrid-scale effects on the filtered flow field, $\bar{\mathbf{u}}^G$. The overbar denotes filtered quantities and the superscript G is used for represented quantities on the LES grid. We define \mathbf{u}^* as our best approximation for the unfiltered field. Stolz *et al.* (2001) and Rembold *et al.* (2001) discussed this in detail and showed that this approach is effective for flow simulations. Thus, it is tempting to ask whether parts of the sound spectrum can also be recovered in an LES.

The source tensor T_{ij} can be decomposed into a part that can be represented on the LES grid (T_{ij}^G) and a part that cannot (T_{ij}^{SG}), just as the velocity field \mathbf{u} is decomposed into a filtered field represented on the grid $\bar{\mathbf{u}}^G$ plus two error terms:

$$T_{ij} = T_{ij}^G(\mathbf{u}) + \underbrace{T_{ij}^{SG}(\mathbf{u})}_{\text{modeled}}, \quad \mathbf{u} = \underbrace{\bar{\mathbf{u}}^G + (\mathbf{u}^G - \bar{\mathbf{u}}^G)}_{\approx \mathbf{u}^*} + (\mathbf{u} - \mathbf{u}^G)$$

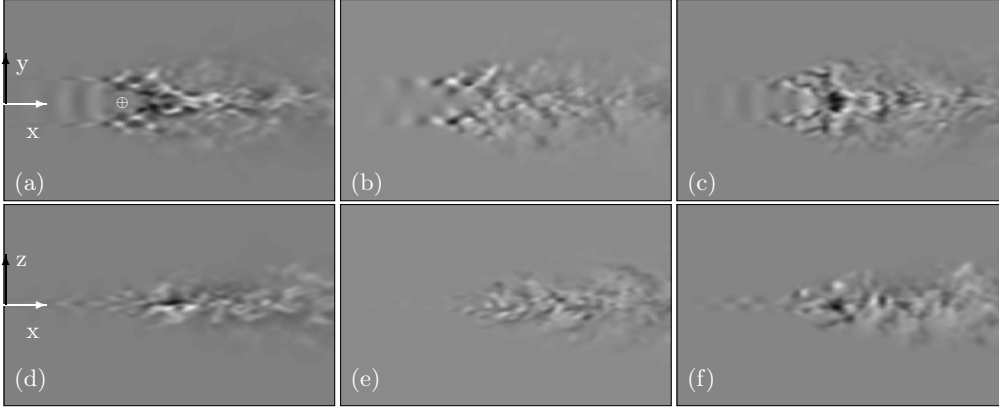


FIGURE 8. Instantaneous contours of T_{11} (a,d), T_{12} (b,e) and T_{13} (c,f) in the major (a-c) and minor (d-f) jet-planes from the LES database, \oplus origin of the far-field arcs.

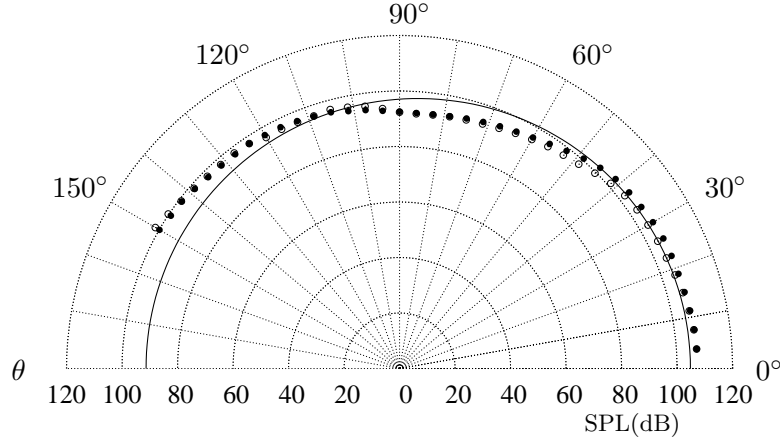


FIGURE 9. Sound pressure level along an arc in the major \circ and minor \bullet jet-plane of radius $60L_1/2$ around the transition area; expected Doppler-scaling — .

We used a five-point explicit filter in computational space with two vanishing moments in physical space. The source tensor components beyond the grid cutoff $T_{ij}^{SG}(\mathbf{u})$ cannot be recovered and must be modeled. These are not considered here. The represented part of the tensor $T_{ij}^G(\mathbf{u})$ is a function of \mathbf{u} but can be evaluated in LES only from the filtered field $\bar{\mathbf{u}}^G$. Seror *et al.* (2001) have shown that the acoustic spectra computed from incompressible homogeneous isotropic turbulence can be improved when the Lighthill stress tensor, based on resolved velocities, is supplemented by the subgrid-scale contribution. In the present study we investigated whether the far-field spectral prediction can be improved when $\bar{\mathbf{u}}^G$ is replaced by $\mathbf{u}^* \approx \mathbf{u}^G$, as is done for the flow computation. First, we computed the far-field sound using $T_{ij}^G(\bar{\mathbf{u}}^G)$ and then compared it with the prediction using deconvolved quantities $T_{ij}^G(\mathbf{u}^*)$. The difference is found to be insignificant, as will

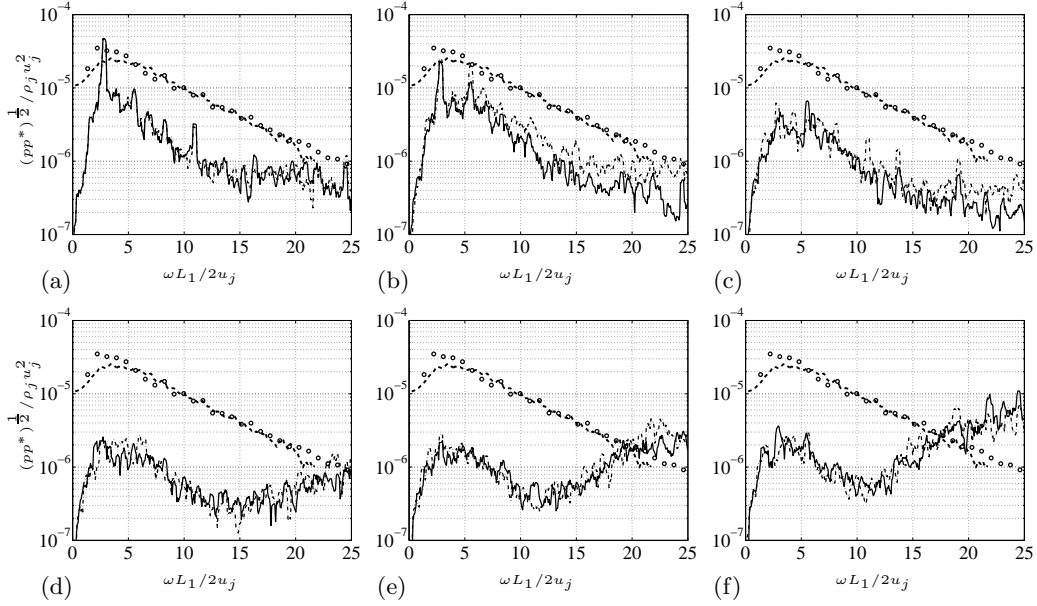


FIGURE 10. Far-field spectra at for the (a) 5° , (b) 30° , (c) 60° , (d) 90° , (e) 120° , (f) 150° , for the arc at radius $60L_1/2$ in the major --- and minor - - - jet-plane. Spectra for a round jet of the DNS of Freund \circ and experiments of Stromberg *et al.* (1980) - - - - at an angle of 30 degrees.

be discussed later. The following results are based on the first formulation of the source term.

The instantaneous source distribution, plotted in figure 8, is seen to be very similar to the distribution in the DNS case (see figure 4) with maximum values at the edges of the jet. Quantitative analysis in the far-field, however, reveals significant discrepancies between the DNS far-field and the LES data (see figures 5 vs. 9). Whereas the directivity in the main radiation direction (at angles around 30 degrees) is well recovered, we observe spurious radiation of the LES jet at higher angles. The far-field spectra show that the spurious noise is at high frequencies, where a rapid increase in the acoustic intensity in the far-field is found, particularly at high angles. For reference the data of Freund (2001) and Stromberg *et al.* (1980) at $\theta = 30$ degrees are again plotted. Careful examination of the origin of these spurious waves is needed and ways to suppress them have to be found.

The same analysis was repeated with the source tensor based on the deconvolved velocities to include the subgrid-scale contribution. We found no significant difference between the results using the two source formulations. At this point it is not clear whether the subgrid-scale contribution is indeed small or is overwhelmed by numerical errors. In order to reliably predict the sound radiation from LES calculations and study the subgrid-scale modeling effects, the source of these spurious waves first needs to be identified and eradicated.

5. Conclusions

We have computed the far-field sound of a Mach 0.5 low-Reynolds-number rectangular jet using a DNS database and Lighthill's acoustic analogy in frequency space, and analyzed the sound pressure level and the frequency spectra along two arcs in the major and minor jet planes. The directivity is found to match the theoretical prediction and the spectra show characteristics similar to comparable data in the literature. In a second step we performed an LES of the same flow using $1/3^3$ the DNS mesh size and again computed the sound. We found that the low frequency part of the far-field spectra is well reproduced by the LES using source formulations based on both the filtered velocities and the approximately deconvolved velocities. However, spurious waves from the LES data resulted in an unphysical increase of the spectral level at higher frequencies, and no subgrid-scale contribution has been observed. For reliable prediction of the far-field sound with compressible LES this spurious effect has to be analyzed further.

REFERENCES

- BASTIN, F., LAFON, P. & CANDEL, S. 1997 Computation of jet mixing noise due to coherent structures: the plane jet case. *J. Fluid Mech.* **335**, 261–304.
- FREUND, J. B. 2001 Noise sources in a low-Reynolds-number turbulent jet at Mach 0.9. *J. Fluid Mech.* **438**, 277–305.
- GOLDSTEIN, M. E. 1976 *Aeroacoustics*. McGraw-Hill, New York.
- GRINSTEIN, F. F. 2001 Vortex dynamics and entrainment in rectangular free jets. *J. Fluid Mech.* **437**, 69–101.
- KINZIE, K. W. & MCCLAUGHLIN, D. K. 1999 Aeroacoustic properties of supersonic elliptic jets. *J. Fluid Mech.* **395**, 1–28.
- NARAYANAN, S., BARBER, T. & POLAK, D. 2000 High subsonic jet experiments. Part II: Turbulence and noise generation studies. *AIAA Paper* 2000-2023.
- REMBOLD, B., ADAMS, N. A. & KLEISER, L. 2001 Direct and large-eddy simulation of a transitional rectangular jet. In *Direct and Large-Eddy Simulation IV* (B. J. Geurts, R. Friedrich & O. Métais, eds.), pp. 197–204. Kluwer, Dordrecht.
- REMBOLD, B., ADAMS, N. A. & KLEISER, L. 2002 Direct numerical simulation of a transitional rectangular jet. *Int. J. Heat and Fluid Flow* **23**, 547–553.
- SEROR, C., SAGAUT, P., BAILLY, C. & JUVÉ, D. 2001 On the radiated noise computed by large-eddy simulation. *Phys. Fluids* **13**, 476–487.
- STOLZ, S. & ADAMS, N. A. 1999 An approximate deconvolution procedure for large-eddy simulation. *Phys. Fluids* **11**, 1699–1701.
- STOLZ, S., ADAMS, N. A. & KLEISER, L. 2001 The approximate deconvolution model for LES of compressible flows and its application to shock-turbulent-boundary-layer interaction. *Phys. Fluids* **13**, 2985–3001.
- STROMBERG, J. L., MCCLAUGHLIN, D. K. & TROUTT, T. R. 1980 Flow field and acoustic properties of a Mach number 0.9 jet at a low Reynolds number. *J. Sound Vibr.* **72**, 159–176.
- YU, M.-H. & MONKEWITZ, P. A. 1990 The effect on nonuniform density on the absolute instability of two-dimensional inertial jets and wakes. *Phys. Fluids* **A2**, 1175–1181.